Productivity, selectivity, and energy consumption of pilot-scale vacuum assisted air-gap membrane distillation for the desalination of high-salinity streams

(Article begins on next page)

18 September 2024

Highlights

- Productivity, selectivity, and energy consumption were investigated in AGMD.

- Feed flow rate and applied vacuum solidly correlate with distillate flux and STEC.

- The distillate quality is regulated by the superposition of vapor and pore flows.

- The total pressure difference across the membrane governs the system rejection.
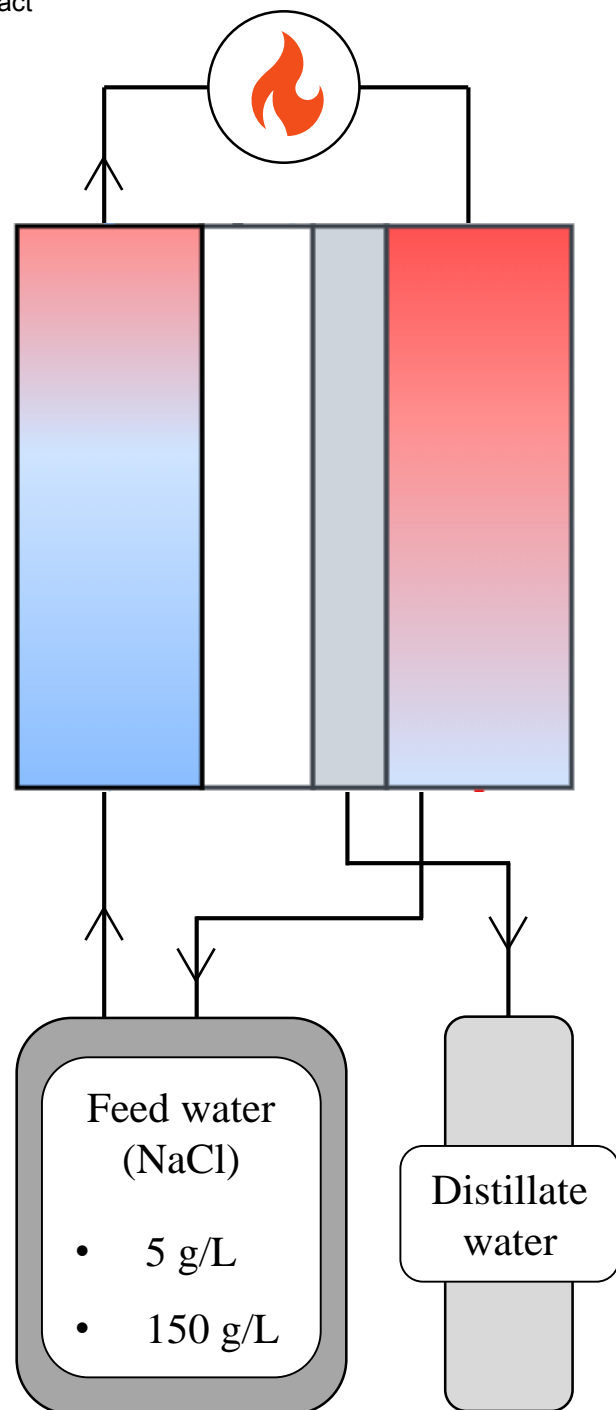
Response Surface Methodology

Productivity | Energy consumption | Selectivity

H$_2$O flux vs vacuum and flow rate

STEC vs vacuum and feed flow rate

Rejection vs total pressure
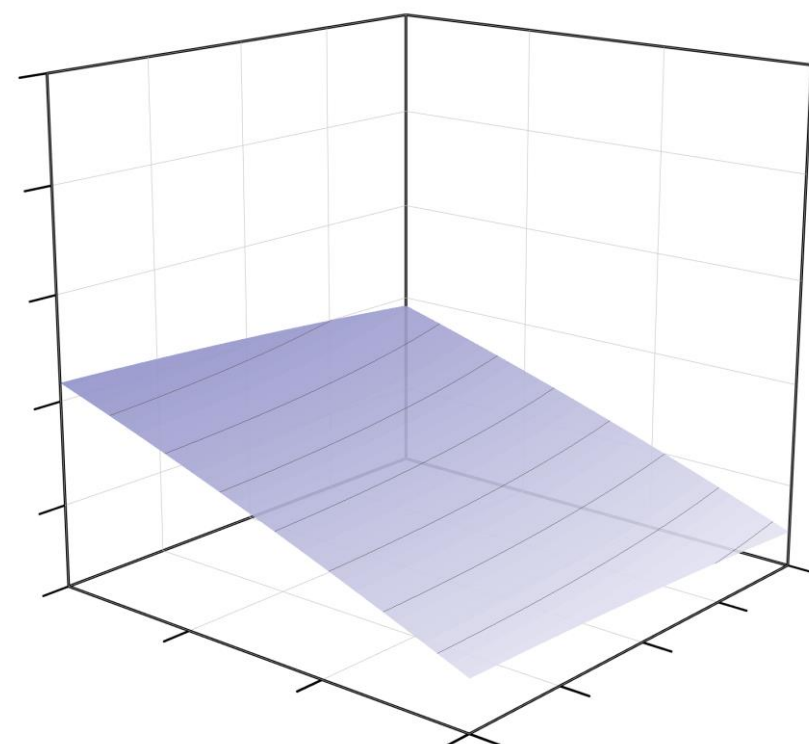
Feed flow rate have an higher impact on distillate flux than applied vacuum
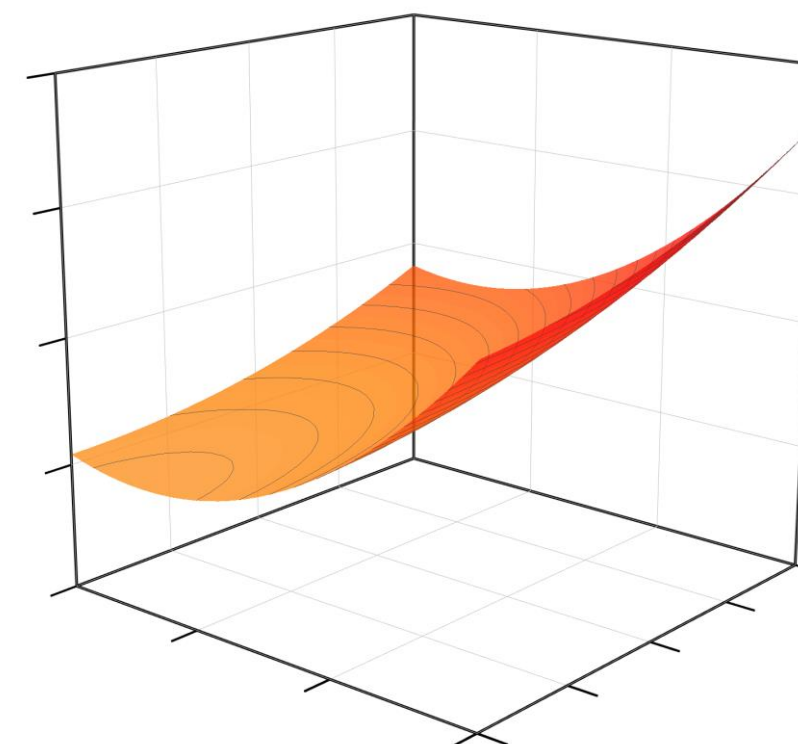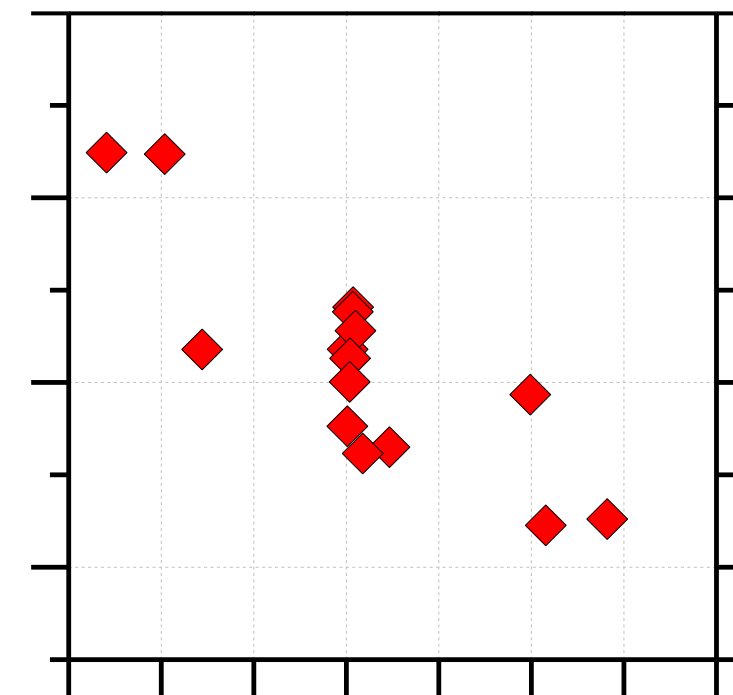
For each vacuum there is a flow rate that minimize the STEC

Decrease in R with total pressure

Feed water (NaCl)
- 5 g/L
- 150 g/L

Distillate water

Productivity, selectivity, and energy consumption of pilot-scale vacuum assisted air-gap membrane distillation for the desalination of high-salinity streams

Marco Malaguti[a], Luke K. Presson[b,c], Alberto Tiraferri[a], Kerri Hickenbottom[b,c], Andrea Achilli[b,c,*]

[a]*Department of Environment, Land and Infrastructure Engineering, Politecnico di Torino, C.so Duca degli Abruzzi 24, 10129, Torino, Italy*
[b]*Department of Chemical and Environmental Engineering, University of Arizona, Tucson, AZ, 85721, United States*
[c]*Water and Energy Sustainable Technology (WEST) Center, University of Arizona, Tucson, AZ, 85745, United States*

Abstract

The implementation of air gap membrane distillation systems is limited by a lack of overall performance predictions which nowadays rely only on few available pilot-scale researches. This study evaluates the productivity, energy consumption, and selectivity of a pilot-scale air gap membrane distillation system by combining experiments and modeling activities. The effect of operating conditions, i.e., applied vacuum, feed flow rate, and feed stream salinity, was investigated to identify regulating factors and quantify dependencies. Response surface methodology was applied to model the phenomena and provide statistical analysis. Increasing flow rates produced a near linear increase of productivity within the investigated range. Working at higher applied vacuum also translated into enhanced productivity, even though the distillate flux increased of maximum 10% when the vacuum value increased from -100 mbar to -500 mbar. The two operating variables also governed the observed salt flux, acting with a similar magnitude to increase it, since salt flux resulted mainly from liquid pore flow phenomena. On the other hand, the total pressure difference across the membrane regulated the membrane rejection: increasing the pressure led to a rejection decrease. Moreover, high feed stream salinity negatively affected both the productivity and the distillate quality. The productivity gains were typically achieved at the expense of an increase in specific thermal energy consumption; however, an interesting relation was observed with feed stream salinity, with a minimum of specific thermal energy consumption of roughly 300 $kWhm^{-3}$ identified in the treatment of a brine with a salinity of 150 gL^{-1}.

Keywords: Air gap membrane distillation; Pilot scale; Performance; Hyper-saline streams; Pore flow.

1. Introduction

The increasing demand for safe freshwater, together with efforts to reduce the impacts of brine management, are leading to the growth of zero liquid discharge (ZLD) strategies and technological solutions [1, 2]. Membrane-based separation processes participate toward achieving ZLD in agricultural, industrial, and desalination applications [3, 4, 5, 6]. In particular, membrane distillation (MD) is gaining interest from both the scientific community and industrial stakeholders, since it can be deployed to attain the desalination of high-salinity streams up to substantial water recovery rates [7, 8, 9]. MD is a thermally-driven process that exploits a temperature difference between the two sides of a hydrophobic membranes

---

*Corresponding author
Email address:* `achilli@arizona.edu` (Andrea Achilli)

to create a vapor pressure difference, which leads to the transport of vapor across the membrane itself. Despite its high energy consumption, MD has higher degree of flexibility in terms of feed salinity in comparison to reverse osmosis desalination and it can be powered with low-grade heat and renewable energy sources [10, 11, 12, 13].

Although a significant amount of research around MD has been carried out in the last decades, full-scale MD systems have not yet reached commercial feasibility, partly due to the fact that pilot-scale investigations aimed at technology scale-up are limited [14]. Technical and economical assessments of MD cannot be accurately performed [15], since the results of numerous bench-scale studies cannot be directly utilized to conduct such analyses. Pilot-scale research is critical to retrieve accurate description of performance and to infer adequate predictions of the behavior of MD systems at full-scale [16, 17]. Among the possible MD configurations, vacuum-enhanced air gap membrane distillation (AGMD) utilizing spiral-wound modules is advantageous in terms of water production and energy efficiency compared to other types of system [18, 19]. The concept underlying vacuum-enhanced AGMD configuration is the increase of distillate water production achievable by exploiting the removal of air (creation of a vacuum) from the gap of the module. This conceptualization was applied in an early stage bench-scale version by Winter et al. in 2011 [20], and subsequently scaled up and commercialized in different configurations by the company Aquastill. A comprehensive evaluation of the AGMD systems should take into account also the energy consumption and the quality of the product water. Several energy analyses have been performed to identify the most efficient configurations, sizes, and sources of exergy losses in AGMD systems [13, 21, 22]. As discussed by Duong et al., the electrical energy consumption in these systems is approximately two order of magnitude lower than the thermal energy [23]. However, both the feed stream salinity and the operating conditions substantially influence the absolute energy needs and the relative contribution of different energy sources. For what concerns the distillate quality, it has been shown that increasing the feed salinity typically worsen the quality of the product water [16, 24]. In terms of operating conditions, Ruiz-Aguirre et al. suggested that the distillate quality may not depend on the operating conditions under ideal conditions, and that the electrical conductivity differences of the permeate that are commonly recorded in experimental investigations may be mainly related to membrane surface defects [14, 25].

In this study, a multi-parameter investigation is presented with the goal to overcome the gap in knowledge on AGMD system behavior and scalability. Specifically, the performance of a pilot-scale vacuum-enhanced AGMD system is discussed considering the productivity of the process, the energy consumption, and the behaviour in terms of product water quality. Response surface methodology (RSM) is applied to model the performance of the investigated MD system [6, 26, 27, 28, 29]. The control variables of the model, i.e., the operating parameters investigated in the experimental campaign, are the feed flow rate, the applied vacuum, and the feed stream salinity (NaCl concentration). On the other hand, the analyzed responses of the model, i.e., the experimental outcomes that can be predicted with statistical significance by the tuned model, are the distillate flux, the temperature difference between the condenser outlet and the evaporator inlet, and the associated specific thermal energy consumption. In addition, the electrical energy consumption is evaluated in comparison to the thermal energy consumption. Seen the limitations of the use of the the absolute distillate quality in correctly describing system selectivity, both membrane rejection and the salt flux are evaluated to achieve a more mechanistic and

2

less system-specific discussion.

2. Materials and methods

2.1. Description of the unit

The experimental campaign was carried out using a pilot-scale vacuum-assisted AGMD system (Aquastill, Sittard, the Netherlands) that was operated at the WEST Center (USA). A schematic of the unit is reported in Fig.1. The pilot setup is essentially composed of a brine circulation loop and separated heating and cooling loops with heat exchangers used to regulate the brine temperature at the inlet of both the cold side ($T_{cold,in}$) and he hot side ($T_{hot,in}$).
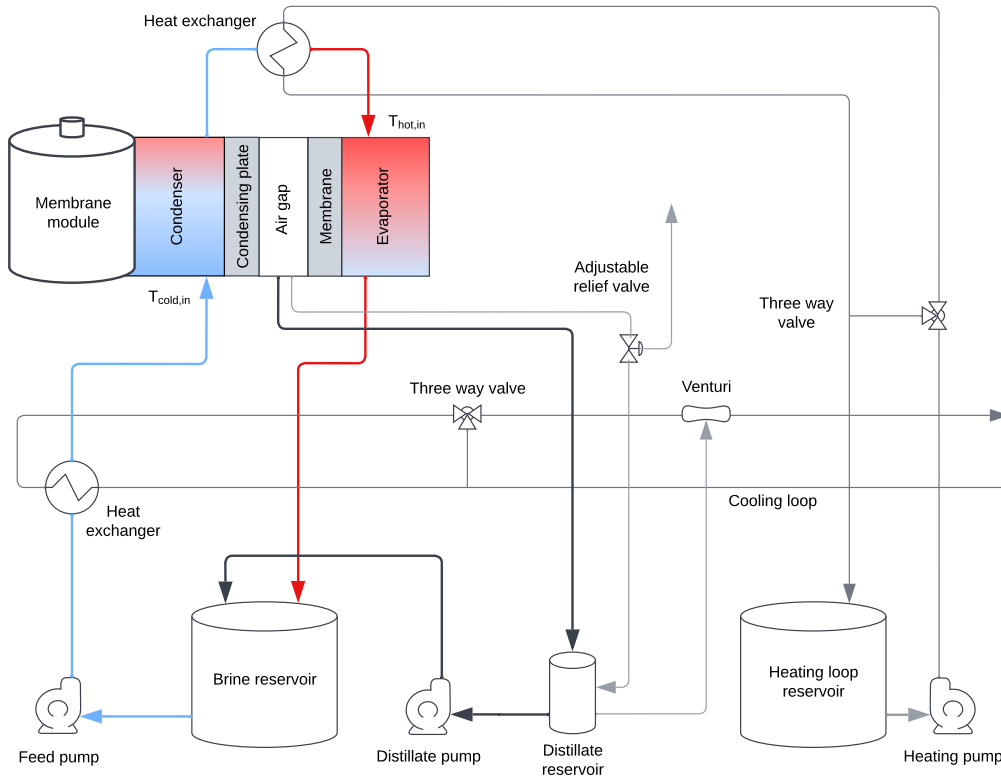

Figure 1: Schematic representation of the experimental pilot system based on vacuum-assisted air-gap membrane distillation. The air gap separates the hot evaporator side and the cold condenser side. The temperature difference between the channels promote the formation of water vapour that permeates through the membrane, condenses on the condenser plate, and it is thus transferred to the cold distillate channel. The water flux in this configuration is enhanced by operating at negative relative pressure in the air gap owing to the vacuum generated by a Venturi tube mounted in-line within the cooling loop.

Thanks to a centrifugal feed pump (Arbo pumps, Smilde, the Netherlands) connected to the brine reservoir, the brine solution first passed through the heat exchanger of the cooling loop to lower its temperature until the set-point was reached in each of the tests (blue line). The cooling loop worked with a constant-flow rate stream of technical water from the tap. The cooling loop was equipped with a section narrowing connected to the permeate collection system (bold line exiting the air gap), which generated a Venturi effect that provided the desired vacuum in the air gap to enhance the vapor transport. After cooling, the brine was fed to the membrane cold channel where the fluid gained sensible heat by conduction from the other membrane side together with latent heat from the vapour re-condensing in the gap. The preheated brine, which

3

served as a gap cooling stream, thus became a preheated feed stream as it exited the cold channel. Its temperature was further increased through a heating loop until the set-point was reached and the hot brine entered the hot feed module channels (red line). The heating loop comprised a submersed coil hosting a flow of technical water heated by an electrical resistance. The difference in vapour pressure due to the temperature gradient between the two sides of the membrane drove the vapor through the membrane pores where condensed distillate was collected in the distillate tank. The brine then exited the hot channels and re-entered the brine tank together with the distillate that was recirculated into the feed tank. In such closed loop configuration, the feed stream concentration was thus maintained almost constant to perform experiments at a fixed salinity value. The vacuum-assisted AGMD unit was equipped with hydraulic pressure sensors at both the hot and the cold inlet and with temperature sensors at the cold inlet, cold outlet, hot inlet, and hot outlet of the brine loop, as well as at the outlet of the distillate channel. All the sensors were monitored by a digital interface and the value recorded by a programmable logic controller (PLC) every 10 seconds. The characteristics of the membrane utilized for this research together with the rejection tested by the manufacturer are reported in Tab. 1.

Table 1: AGMD module and membrane characteristics.

Parameter	Unit	Value
Membrane material	-	Polyethylene
Number of channels	-	12
Membrane active area	m^2	25.92
Channel length	m	2.7
Nominal pore size	μm	0.3
Thickness	μm	96
Porosity	%	85
Manufacturer measured rejection	%	99.75

2.2. AGMD performance estimators

The performance of the AGMD system was evaluated in terms of productivity, STEC, specific electrical energy consumption (SEEC), and salt flux (J_s). All experiments were performed at constant $T_{hot,in}$ and $T_{cold,in}$ equal to 70 $°C$ and 30 $°C$, respectively. Variables were recorded always under steady-state conditions to ensure reliability of the performance in long-term operations. To ensure that the steady-state was reached, each experiment was performed for a duration of at least 6 hours [30]. All the experiments were performed at 0% water recovery, i.e. the distillate water was continuously recirculated into the brine tank. The productivity of the unit was assessed by computing J_w, the water flux across the membrane, as given in Eq.1.

$$J_w = \frac{V_{d.t}}{A \cdot t} \tag{1}$$

where A is the active area of the membrane and $V_{d.t}$ is the volume of distillate collected in the time frame t. Both the thermal and the electrical energy consumption was assessed. The thermal analysis was performed analyzing the STEC, which is widely used since it expresses the external thermal energy input necessary to produce one cubic meter of distillate

4

water. The STEC was computed according to Eq.2.

$$STEC = \frac{Q_f \cdot \rho_f \cdot C \cdot (T_{hot,in} - T_{cold,out})}{J_w \cdot A \cdot 3.6 \cdot 10^6} \qquad (2)$$

where Q_f is the feed flow rate, ρ_f is the feed density, and C is the specific heat capacity that is assumed to be constant. The SEEC indicates instead the electrical energy consumed per volume unit of distillate product and was calculated using Eq.3.

$$SEEC = \frac{Q_f \cdot \Delta P_{drop}}{36 \cdot \eta \cdot J_w \cdot A} \qquad (3)$$

where ΔP_{drop} is the hydraulic pressure drop over the membrane module and η the efficiency of the water-circulating pump. The salt passing through the hydrophobic membrane was attributed to the pore flow phenomenon that can be associated with 'defects' that allow convective flow of water in the liquid phase [31]. That is, all other mechanisms producing a salt passage across the membrane were considered negligible compared to the pore flow effect. In the presence of pore flow, the total water flux is the sum of both the vapor flux and the liquid flux. With the assumption that pore flow is a linear function of the trans-membrane pressure difference, similarly to membrane processes working with hydrophilic membranes, the total water flux was thus calculated as:

$$J_w = J_{w,v} + J_{w,l} = \beta \Delta P_v + L_d \Delta P \qquad (4)$$

where $J_{w,v}$ and $J_{w,l}$ are the vapor flux and the liquid flux, respectively, β is the membrane permeability, ΔP_v is the vapor pressure difference across the membrane, ΔP is the trans-membrane hydraulic pressure difference, and L_d is the permeability associated with membrane defects. When pore flow occurs, non-volatile solutes are also transported across the membrane in the liquid phase. The salt flux J_s was evaluated as a function of either the total water flux or the liquid water flux as:

$$J_s = J_w \cdot c_d = J_{w,l} \cdot c_f \qquad (5)$$

where c_d and c_f are the concentrations of NaCl in the distillate product and in the feed stream, respectively. It is worth highlighting that the solution conductivity was measured instead of the salt concentration, since the former can be used as proxy for the latter within concentration ranges whereby the two parameters have a linear relationship. As extensively discussed in previous literature studies, this relationship may be confidently assumed to be linear at values of salt concentration lower than approximately 150 g/L [14]. The correlation is reported in Fig.S1 in the Supporting Information (SI). The last parameter used to evaluate the selectivity of the process is the log rejection calculated according

5

to the Eq.6.

$$Log_{10}Rejection = Log_{10}\left(1 - \frac{c_d}{c_f}\right) \tag{6}$$

Electric conductivity was used as av proxy for salt concentration. Therefore, in Eq.6 c_f is the electric conductivity measured in the feed tank, which may be considered constant because the experiments were performed under near steady-state conditions with both the concentrate and the distillate streams being recirculated into the feed tank. c_d is instead the average electric conductivity values measured in the distillate pipe exiting the module throughout the test. The distillate stream electric conductivity was practically constant (low standard deviation) during each test, owing to steady-state conditions. Note that c_f represents the inlet bulk feed conductivity, not the average bulk conductivity of the salty stream in the evaporator channel, the latter increasing along the module as water recovery increased, while c_d represents the conductivity from the distillate flow coming from the entire module. Therefore, rejection calculated with Eq.6 should be rigorously regarded as an observed "module rejection" rather than an observed "membrane rejection", which would require associating c_d with the average bulk conductivity of the salty stream within the module. That being said, since the recovery rate of the module was small, typically between 1 and 3% for the various tests and always <4%, the change in c_f or c_d along the module may be considered negligible and the results obtained by applying Eq.6 may be interpreted in this study as "membrane rejection" values for all practical purposes.

2.3. Design of experiments, statistical analyses, and experimental procedures

The software Design Expert was used to design the experimental campaign based on RSM through the application of the CCD, which defined the number of experiments and the values of the variables needed for the statistically significant assessment of the variables and responses. In addition, the experimental campaign was conducted for three different NaCl feed salinities: 1, 5, 150 g/L. The Supplementary material appendix presents further details of the applied CCD method and analyses. The statistical ranges of variable values are reported Tab. 2, together with the experimental ranges necessary to properly build the response surface through CCD and to probe the entire multidimensional space. In this scenario, 13 experiments were performed for each salinity, 8 of them at different values of flow rate and vacuum, together with 5 replicates of the central point, for a total of 39 experiments for the overall research study.

Table 2: Experimental design of the selected operating conditions, representing the range of variable values of the RSM model.

Controls	Unit	Modeling range	Experimental range
Vacuum	mbar	100 - 500	17 - 583
Feed flow rate	L h^{-1}	600 - 1200	476 - 1324

The collected experimental results were used as input data to generate the model for each response according to the best quadratic fit. Analysis of variance (ANOVA) was used to analyze the statistics and to evaluate the quality of the obtained model.

3. Results and discussion

3.1. Relationship between applied vacuum, feed flow rate, and productivity

The steady-state distillate flux observed in the experiments is reported against feed flow rate and the vacuum value in Fig.2. An increase in feed flow rate always translated into higher distillate fluxes, i.e. productivity, regardless of the vacuum value. This trend was described also in a research report by Eykens et al. [32] and in a review by Chen et al. [33]. Also an increase in the applied vacuum led to greater productivity, while the impact of this second operating variable was substantially lower than that of feed flow rate. These trends are well exemplified by comparing the results of the various experiments performed at 100 mbar with those obtained at 500 mbar vacuum, under the same feed flow rate values. While doubling the feed flow rates translated into a similar increase in water flux, working at a vacuum value five times higher only resulted in marginally larger productivity, up to roughly 10% of gain; see Fig.2, second and fourth panel. In previous research, Liu et al. [34] suggested that even if an increase in vacuum inside the air gap lowered the resistance in the pores while enhancing the vapor pressure difference and therefore of the exploited driving force, the recorded productivity improvements were barely more than 10%. The data plotted in Fig.2 also imply that feed stream salinity is an important factor regulating productivity, since the distillate flux in the hyper-saline scenario (150 g/L) was substantially lower than that observed in the low and medium salinity cases (1 g/L, 5 g/L). For this reason, and due to the strong similarity between the results obtained at 1 g/L and 5 g/L, the following sections will only discuss results related to 5 g/L and 150 g/L feed stream salinities. In summary, the observed productivity were coherent with available literature studies performed with similar configurations, modules size, as well as evaporator and condenser temperatures [18, 31, 24, 23, 26**?** , 35]. Specifically, distillate fluxes between 0.5 $Lm^{-2}h^{-1}$ and 2.5 $Lm^{-2}h^{-1}$ were observed for low to medium salinity scenarios while fluxes lower than 1.5 $Lm^{-2}h^{-1}$ were typically measured when dealing with a hyper-saline feed stream ($c_f = 150 \ gL^{-1}$).

Based on the flux results discussed just above, the response surfaces were built for the low salinity scenario (Fig.3a) and for the hyper-saline scenario (Fig.3b). The graphs report the surface of the distillate flux values modeled as a function of feed flow rate and applied vacuum. Despite absolute values being substantially higher for the low salinity feed, the two surfaces present analogous shape that supports the reliability of the results and confirms that the impact of feed flow rate was dominant compared to that of applied vacuum. This might be due to the decrease of both temperature and concentration polarization effects associated to increased feed flow rates [23]. On the other hand, the loss in productivity due to salinity accounts for a decrease of around 50% between the two cases, as similarly shown in previous research [24]. Moreover, it is worth mentioning that the surface in Fig.3a shows a minimum flux ad mid vacuum values. This might be suggesting that the decrease in temperature difference when increasing the applied vacuum (as observed in Fig.4a and discussed in the next paragraph) generates a decrease in driving force that is more significant than the lowered resistance in the pores due to vacuum increase itself, until around 300mbar when the latter effect becomes dominant. However, these pilot-scale results and their absolute values of distillate flux suggest that in a real scale operation an increase in productivity would be more easily pursued by selecting a larger feed flow rate instead of enhancing the applied vacuum.
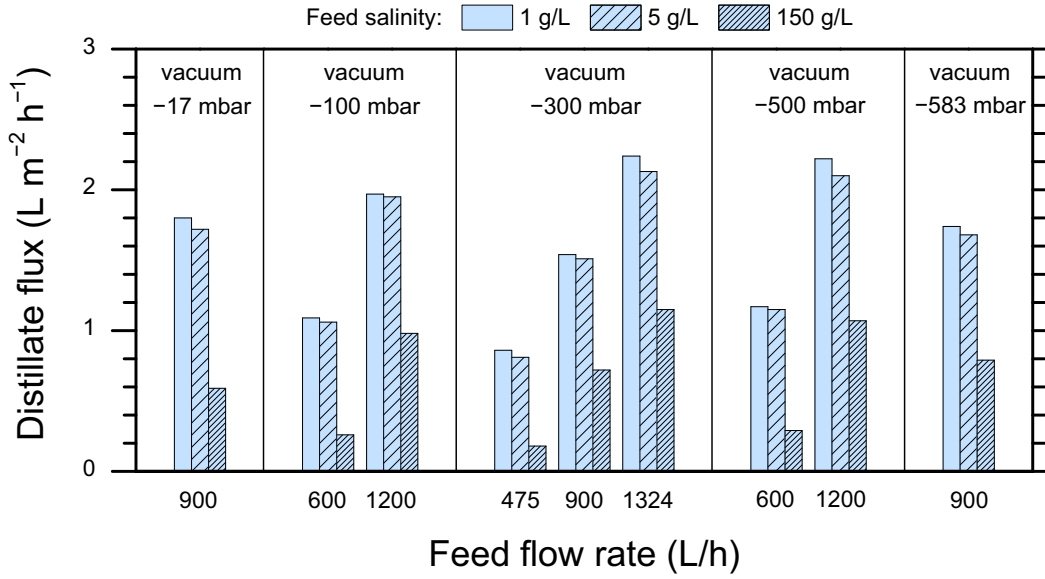
7

Figure 2: Steady-state distillate flux (y-axis) is reported as a function of feed flow rate (x-axis) and of vacuum value. The solid bars refer to feed stream containing 1 g/L of NaCl, the sparsely patterned bars refer to a feed stream containing 5 g/L of NaCl, while the densely patterned bars are related to a concentration of 150 g/L. These data are those used to build the respond surface for the distillate flux. For the central point, i.e. Q_f equal to 900 L/h and applied vacuum equal to -300 mbar, the five replicates showed negligibly different results, i.e., within 2%, and for this reason standard deviation bars cannot be observed, although present in the graph.

In addition, it is worth noting that both surfaces present a pseudo-linear behavior. This observation implies that the performance improvement obtained by increasing the operating parameters may be considered largely independent of the initial conditions.
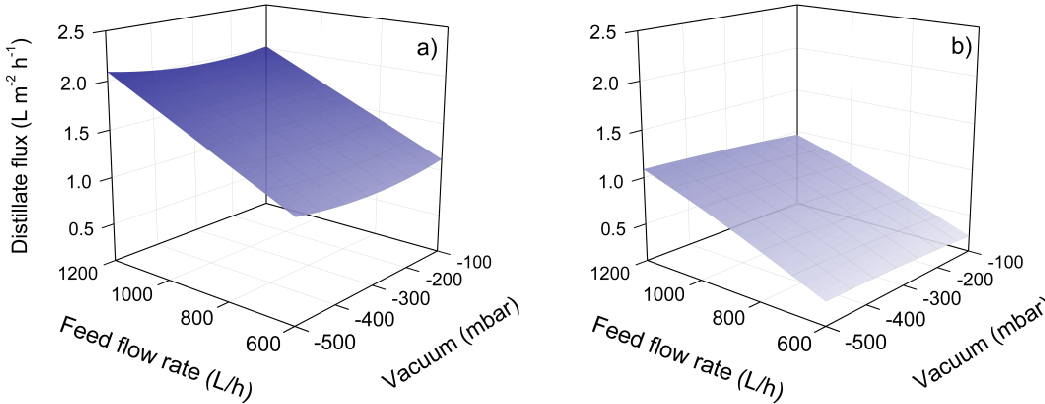

Figure 3: Modeled distillate flux values are reported as a function of vacuum and feed flow rate. Figure a) refers to a feed solution with 5 g/L of NaCl while in b) the feed concentration is 150 g/L. The surface shade has visual purpose only, and it does not refer to a quantitative flux scale.

3.2. Relationship between applied vacuum, feed flow rate, and energy consumption

In general, according to the definition of STEC reported in Eq.2, an increase in distillate flux, a decrease in feed flow rate, and/or a decrease in the temperature difference between the cold outlet and the hot inlet, translate into a lower specific thermal energy consumption. The energy performance of the process lies on the trade-off behavior of these various parameters and their relative impacts. To address these phenomena, the response surfaces were firstly built for the

8

temperature difference between the evaporator inlet and the condenser outlet. The obtained results are reported in Fig.4.
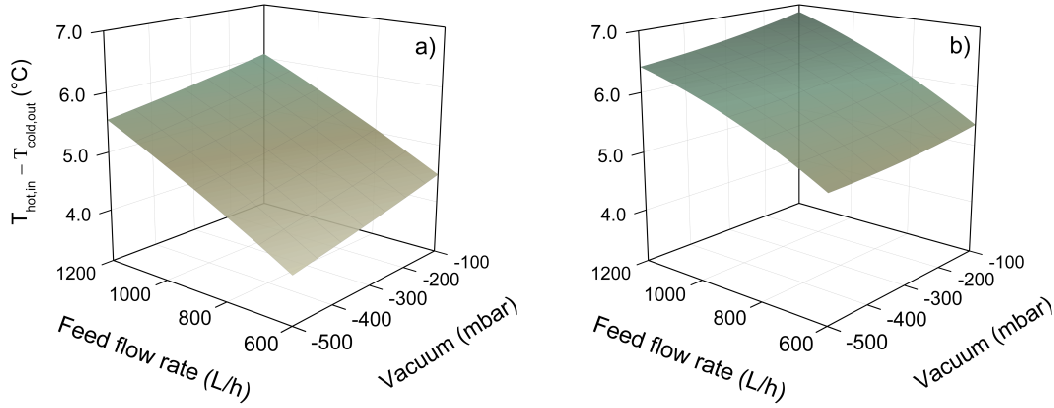

Figure 4: Temperature difference between the feed hot inlet and the feed cold outlet, modeled as a function of vacuum and feed flow rate. Figure a) refers to a feed solution with 5 g/L of NaCl while in b) the concentration was 150 g/L. This temperature difference influences the specific thermal energy consumption, since it is proportional to the amount of heat that the heat source needs to transfer to the feed stream to reach the target feed temperature. The surface shade has visual purpose only, and it does not refer to a quantitative scale.

Analogous trends of temperature difference were recorded for both the two investigated feed salinity. The modeled surfaces highlight that an increase in feed flow rate would always translate into an increase in temperature difference between the cold outlet and the hot inlet (and thus into a larger STEC), while an increase in the applied vacuum would lead to a decrease in the temperature difference and thus to STEC reduction. It is important to point out that at high salinity values the effect of applied vacuum becomes small according to the model, and that the dominant regulating factor remains the feed flow rate. In general terms, as previously discussed by Hardikar et al. [8], when dealing with pilot scale AGMD systems, the effective trans-membrane temperature difference, i.e. the driving force, is roughly one order of magnitude lower than the one related to the set hot and cold inlet temperatures. Typical values of temperature difference lie between $3°C$ - $7°C$ when condenser and evaporator inlets are set at $30°C$ and $70°C$, respectively. This mechanism is the main reason for the relatively low distillate fluxes recorded in this research (see Fig.2 and Fig.3) and in all the other pilot scale studies, especially when compared to bench-scale results.

The trends in temperature difference may be rationalized considering the various heat flow mechanisms occurring across the membrane and within the channels. An increase in feed flow rates always produces an increase in the temperature difference between the two membrane sides and thus generates also a substantial higher vapor fluxes, i.e. productivity. However, increasing the feed flow rate also lowers the feed residence time in the flow channel, consequently reducing the heat transfer between the two membrane sides and diminishing thus the brine preheating [35]. The decrease in temperature difference when increasing vacuum values may be attributed to the latent heat flux combined with the effect of enhanced convective heat flux within the air gap, both sustaining the heat transfer between the condensing distillate and the cold feed side of the membrane, thus increasing the temperature of the latter. These mechanisms seemed to be substantially thwarted in the hyper-saline scenario, whereby the distillate flux was strongly reduced.

The trends in distillate flux and temperature difference discussed above translated into consequential results in terms STEC as a function of operating conditions and feed salinity. First of all, note that the modeled STEC values differ in
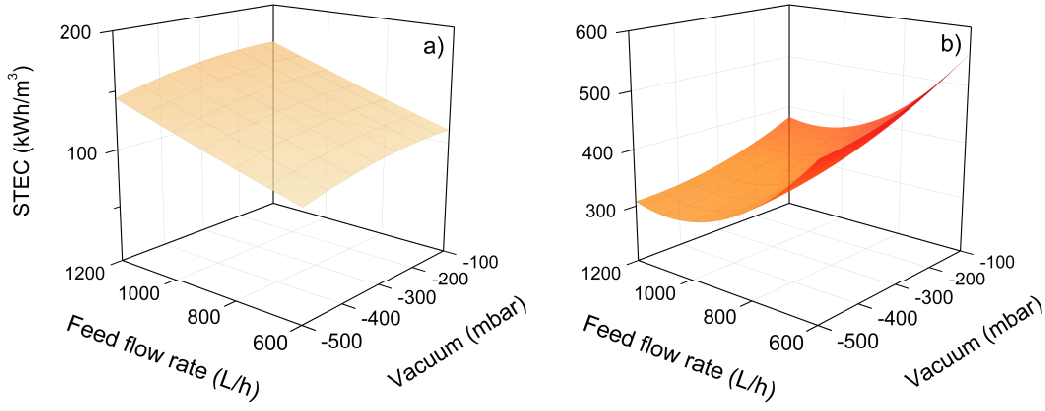
9

Figure 5: Specific thermal energy consumption obtained as a function of applied Vacuum and feed flow rate. Figure a) is referring to a feed solution with 5 g/L of NaCl while in b) the concentration was 150 g/L.The color has visual purpose only, and it does not refer to a quantitative scale.

orders of magnitude in Fig.5a) and b) (the color scale is the same while the z-axis is different to properly show the surfaces shapes). For the low-salinity case, a trade-off between productivity and STEC was observed when changing the feed flow rates: increasing this parameter was detrimental from the perspective of thermal energy consumption (Fig.5 a), but it led to a distillate flux increase (Fig.3a). However, according to Eq.2, the higher achieved productivity was not sufficient to counteract the combined negative effects of higher temperature difference and higher feed flow rate itself on specific energy consumption, which was higher as a consequence. On the other hand, increasing the magnitude of the vacuum would only produce negligible effects on productivity and a slight decrease in STEC.

For the hyper-saline scenario reported in Fig.5b), a completely different trend can be observed: according to the modeled surface, an increase in vacuum would translate into both an increase in distillate flux and into a decrease in temperature difference. These combined effects produced a substantial decrease in STEC, hence an improvement in both productivity and thermal energy performance, indeed at the expense of higher electrical energy use. When considering the influence of feed flow rates, a non-monotonous trend was modeled, with the STEC decreasing with feed flow rates and reaching a shallow minimum around 1000 L/h. To the best of our knowledge, a similar shape was previously recorded only in a research by Winter et al. [20] and modelled by Swaminathan et al. [13] and by Hardikar et al. [35]. This result implies that when dealing with a hyper-saline stream a system optimization is possible and that an optimal feed flow rate exists that would increase the productivity while minimizing the specific thermal energy consumption of the process. On the other hand, in a low-salinity case, the STEC is always lowered when decreasing the feed flow rate. In summary, as discussed by Hardikar et al. [35], the flow rate that minimizes the STEC is zero at zero salinity, and it increases as the salinity increases as showed in the results of Fig.5.

To account for the overall energy consumption of the process, the SEEC was evaluated for selected experiments. It is well known that in MD the electrical energy consumption necessary to pump the water trough the membrane channels is orders of magnitude lower than the thermal energy consumption, as shown in Fig.6 and as corroborated by recent publications [23, 26]. This fact simply implies that, except when AGMD systems are powered by abundant waste heat sources, the minimization of the overall specific energy consumption (SEC) should be performed focusing only on the
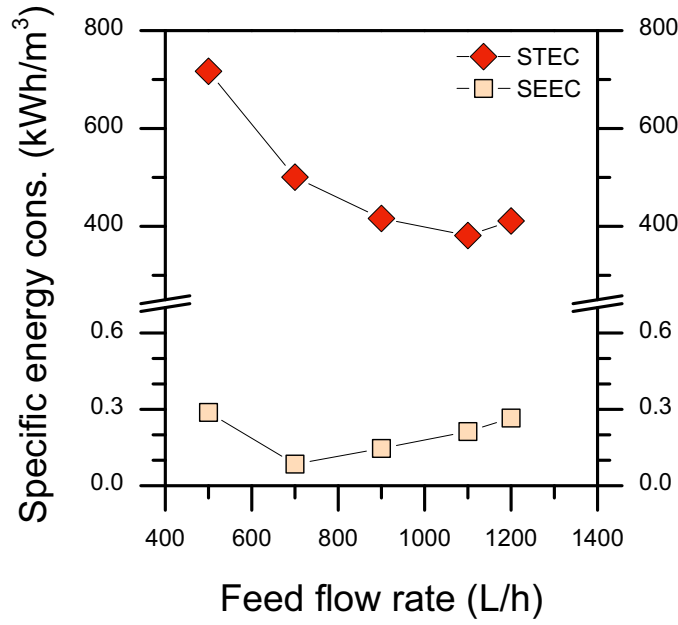
10

Figure 6: Specific energy consumption (SEC) is plotted against flow rate at a fixed applied vaccum of 300 mbar and at a concentration of 150 g/L of NaCl. In particular, both the two components of SEC, i.e. the specific thermal energy consumption (STEC) and specific electric energy consumption (SEEC), are reported. The pump efficiency has been assumed equal to 70% to give a conservative estimation. The lines connecting the symbols are used only as a guide for eyes.

thermal contribution since, according to the experiments of this research, the latter accounts for 99.95% of the overall energy consumption.

3.3. Quality of the product distillate water: vapor and pore flows

While it is consolidated that the distillate quality depends on the operating conditions, e.g., vacuum, flow rate, salinity, temperatures, the prediction of AGMD systems selectivity is still challenging, especially in hyper-saline scenarios [14, 18, 24]. One parameter that could unravel the selectivity of the process is the salt flux. The results obtained in this study in terms of salt flux are reported in Fig.S2 in the Supporting Information (SI). In summary, Fig.S2 illustrates that an increase in feed flow rate or in applied vacuum always translates into a larger salt flux. This phenomenon may be rationalized with the higher hydraulic pressure difference between the two membrane sides, which is the parameter regulating the pore flow [14, 24, 31]. However, salt flux alone cannot fully explain the selectivity behavior of the membrane itself and it is not necessarily a reliable predictor of distillate quality, since salt flux is dependent on water flux (see Eq.5), a correlation that was corroborated experimentally in this study; see Fig.S2. Salt rejection should be instead evaluated to obtain a full understanding of selectivity.

The rejection results obtained in this study are reported in Fig.7 where the log of rejection is plotted against the hydraulic pressure difference. The rejection was high in all the tests and above 99.1% (above 2-$\log_{10}$). Nevertheless, the data highlight that the rejection of the membrane was consistently lower when the feed stream contained high salt concentration, especially at low values of the hydraulic pressure difference. This may be explained by the decrease in water flux when increasing the feed stream that directly translates into a rejection decrease [7, 14]. Moreover, the plots suggest that the rejection was largely regulated by the hydraulic pressure difference across the membrane. As reported in Tab.3, the
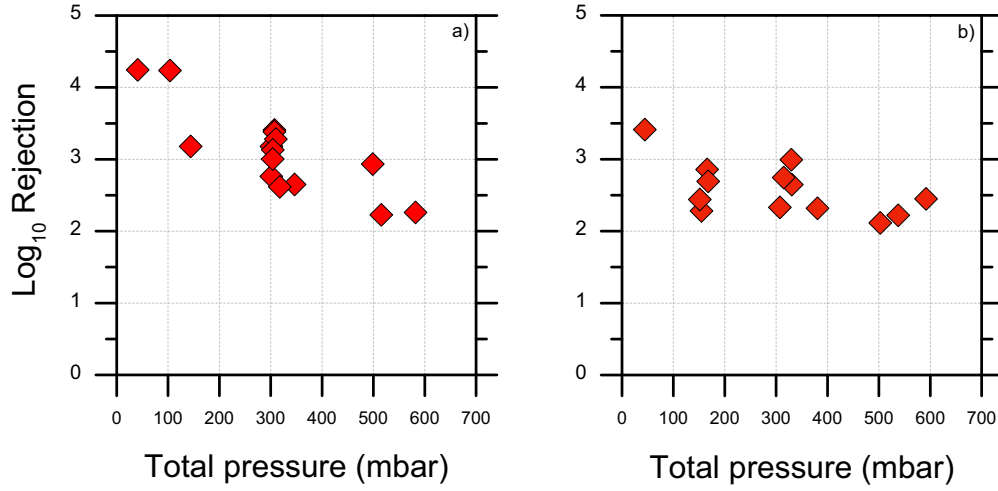
11

Figure 7: Evaluation of selectivity behavior of the process. The log of rejection is reported as a function of the average hydraulic pressure across the membrane: average channel pressure plus applied vacuum. Panel a) shows data relative to the feed stream containing 5 g/L of NaCl, while panel b) refers to the feed stream containing 150 g/L of NaCl.

hydraulic pressure difference is calculated as the sum of the applied vacuum and of the average pressure of the evaporator channel between the inlet and the outlet, the latter related to the feed flow rate. Note that the impact of applied vacuum on the hydraulic pressure was dominant in this study and thus it may be regarded as the main parameter regulating salt rejection. Pressure data related to the 150 g/L salinity are reported in Tab.S1.

Table 3: Operating conditions and resulting average hydraulic pressure difference across the membrane when operating at 5 g/L feed salinity. The evaporator pressure column refers to the average hydraulic pressure into the channel.

Applied vacuum (mbar)	Feed flow rate (L h^{-1})	Evaporator pressure (mbar)	Total pressure (mbar)
295	900	12	307
299	476	2	301
295	900	12	307
291	1324	56	347
298	900	12	310
292	900	13	304
99	1200	45	144
101	600	3	104
496	600	2	499
478	1200	37	515
19	900	21	41
573	900	9	582
291	900	10	301
305	476	2	308
301	476	3	304

4. Conclusion

Air gap membrane distillation represents a promising technology for the concentration of hyper-saline streams achieving near zero liquid discharge. However, further implementation of this technical strategy can be thwarted since only few researches dealing with the scalability and the behavior of pilot and full-scale AGMD systems have been recently published.

12

This research unraveled the effect of feed stream salinity and operating conditions (i.e. feed flow rate and applied vacuum) on productivity, energy consumption, and selectivity of a pilot-scale AGMD system. In summary, the main findings of this study are: i) feed flow rate had a stronger impact on water flux than applied vacuum even if an increase in both led to higher productivity. ii) When a hyper-saline brine was used as feed stream, the productivity decreased drastically compared to feed solutions characterized by low salinity. iii) The specific thermal energy consumption increased pseudo-linearly with feed flow rate at low salinity values while in an hyper-saline scenario when increasing the feed flow rate a decrease in STEC was observed (a minimum value of STEC can be identified). iv) When increasing the feed flow rate and/or the applied vacuum, the salt flux increased and the rejection decreased, thus worsening the quality of the distillate product. Data suggest that the salt rejection was regulated by the hydraulic pressure difference across the membrane: an increase in pressure translated into a decrease in rejection. The results indicate that an increase in feed flow rate led to an improvement in the productivity with a consequent increase in salt flux. On the other hand, an increase in vacuum led to a slight increase in water flux and thus to a more effective preheating phase that together translate into an system energy performance improve. In addition, vacuum dominated also the hydraulic pressure difference across the membrane and thus its increase lowered consistently the salt rejection.

Nomenclature

Acronyms

AGMD	Air gap membrane distillation
ANOVA	Analysis of variance
CCD	Central composite design
LEP	Liquid entry pressure
MD	Membrane distillation
PLC	Programmable logic controller
RO	Reverse osmosis
RSM	Response surface methodology
ZLD	Zero liquid discharge

Symbols

β	$L \cdot m^{-2} \cdot h^{-1} \cdot bar^{-1}$, membrane vapor permeability
ΔP	bar, trans-membrane hydraulic pressure difference
ΔP_v	bar, vapor pressure difference across the membrane
ΔP_{drop}	bar, hydraulic pressure drop over the membrane module
η	$-$, efficiency of the water-circulating pump
ρ_f	$kg \cdot m^{-3}$, feed density
A	m^2, membrane active area

13

C	$J \cdot kg^{-1} \cdot^\circ C^{-1}$, specific heat capacity
c_d	$g \cdot L^{-1}$, concentration of NaCl in the produced distillate
c_f	$g \cdot L^{-1}$, concentration of NaCl in the feed stream
J_s	$g \cdot m^{-2} \cdot h^{-1}$, salt flux
J_w	$L \cdot m^{-2} \cdot h^{-1}$, total water flux
$J_{w,l}$	$L \cdot m^{-2} \cdot h^{-1}$, liquid water flux
$J_{w,v}$	$L \cdot m^{-2} \cdot h^{-1}$, vapor water flux
L_d	$L \cdot m^{-2} \cdot h^{-1} \cdot bar^{-1}$, permeability associated with the membrane defects
Q_f	$m^3 \cdot h^{-1}$, feed flow rate
$T_{cold,in}$	$^\circ C$, cold inlet temperature
$T_{cold,out}$	$^\circ C$, cold outlet temperature
$T_{hot,in}$	$^\circ C$, hot inlet temperature
$T_{hot,out}$	$^\circ C$, hot outlet temperature
$V_{d,t}$	$L \cdot h^{-1}$, volume of distillate collected in the time t
SEEC	$kWh \cdot m^{-3}$, specific electrical energy consumption
STEC	$kWh \cdot m^{-3}$, specific thermal energy consumption

Competing Interests

The Authors declare no Competing Financial or Non-Financial Interests.

Data availability

The data generated during the current study are available from the corresponding author on request.

Author contribution

M. M.: Conceptualization, Formal analysis, Investigation, Data curation, Writing - original draft

L. K. P.: Methodology, Formal analysis, Investigation, Writing - review & editing.

A. T.: Funding acquisition, Supervision, Visualization, Writing - review & editing.

K. H.: Funding acquisition, Project administration, Resources, Supervision, Writing - review & editing.

A. A.: Funding acquisition, Project administration, Resources, Supervision, Writing - review & editing.

14

References

[1] L. K. Presson, V. Felix, M. Hardikar, A. Achilli, K. L. Hickenbottom, Fouling characterization and treatment of water reuse concentrate with membrane distillation: Do organics really matter, Desalination 553 (2023) 116443.

[2] T. Tong, M. Elimelech, The global rise of zero liquid discharge for wastewater management: Drivers, technologies, and future directions, Environ. Sci. Technol. 50 (13) (2016) 6846–6855.

[3] C. A. Quist-Jensen, F. Macedonio, E. Drioli, Membrane technology for water production in agriculture: Desalination and wastewater reuse, Desalination 364 (2015) 17–32.

[4] F. Ricceri, M. Malaguti, C. Derossi, M. Zanetti, V. Riggio, A. Tiraferri, Microalgae biomass concentration and reuse of water as new cultivation medium using ceramic membrane filtration, Chemosphere 307 (2022) 135724.

[5] V. Yangali-Quintanilla, Z. Li, R. Valladares, Q. Li, G. Amy, Indirect desalination of red sea water with forward osmosis and low pressure reverse osmosis for water reuse, Desalination 280 (1) (2011) 160–166.

[6] M. Malaguti, L. Craveri, F. Ricceri, V. Riggio, M. Zanetti, A. Tiraferri, Dewatering of scenedesmus obliquus cultivation substrate with microfiltration: Potential and challenges for water reuse and effective harvesting, Engineering (2023).

[7] R. Schwantes, L. Bauer, K. Chavan, D. Dücker, C. Felsmann, J. Pfafferott, Air gap membrane distillation for hypersaline brine concentration: Operational analysis of a full-scale module–new strategies for wetting mitigation, Desalination 444 (2018) 13–25.

[8] M. Hardikar, I. Marquez, A. Achilli, Emerging investigator series: membrane distillation and high salinity: analysis and implications, Environ. Sci. Water Res. Technol. 6 (6) (2020) 1538–1552.

[9] A. L. McGaughey, A. E. Childress, Wetting indicators, modes, and trade-offs in membrane distillation, J. Membr. Sci. 642 (2022) 119947.

[10] M. R. Qtaishat, F. Banat, Desalination by solar powered membrane distillation systems, Desalination 308 (2013) 186–197.

[11] M. Inkawhich, J. Shingler, R. S. Ketchum, W. Pan, R. A. Norwood, K. L. Hickenbottom, Temporal performance indicators for an integrated pilot-scale membrane distillation-concentrated solar power/photovoltaic system, Appl. Energy 349 (2023) 121675.

[12] M. Malaguti, A. F. Novoa, F. Ricceri, M. Giagnorio, J. S. Vrouwenvelder, A. Tiraferri, L. Fortunato, Control strategies against algal fouling in membrane processes applied for microalgae biomass harvesting, J. Water Process. Eng. 47 (2022) 102787.

[13] J. Swaminathan, H. W. Chung, D. M. Warsinger, J. H. Lienhard V, Energy efficiency of membrane distillation up to high salinity: Evaluating critical system size and optimal membrane thickness, Appl. Energy 211 (2018) 715–734.

[14] A. Ruiz-Aguirre, J. A. Andrés-Mañas, G. Zaragoza, Evaluation of permeate quality in pilot scale membrane distillation systems, Membranes 9 (6) (2019).

[15] A. Tiraferri, M. Malaguti, M. Mohamed, M. Giagnorio, F. J. Aschmoneit, Standardizing practices and flux predictions in membrane science via simplified equations and membrane characterization, npj Clean Water 6 (1) (2023) 58.

[16] E. Guillén-Burrieza, G. Zaragoza, S. Miralles-Cuevas, J. Blanco, Experimental evaluation of two pilot-scale membrane distillation modules used for solar desalination, J. Membr. Sci. 409-410 (2012) 264–275.

[17] A. Ruiz-Aguirre, J. A. Andrés-Mañas, J. M. Fernández-Sevilla, G. Zaragoza, Experimental characterization and optimization of multi-channel spiral wound air gap membrane distillation modules for seawater desalination, Sep. Purif. Technol 205 (2018) 212–222.

[18] J. A. Andrés-Mañas, I. Requena, G. Zaragoza, Characterization of the use of vacuum enhancement in commercial pilot-scale air gap membrane distillation modules with different designs, Desalination 528 (2022) 115490.

[19] L. Francis, F. E. Ahmed, N. Hilal, Advances in membrane distillation module configurations, Membranes 12 (1) (2022).

[20] D. Winter, J. Koschikowski, M. Wieghaus, Desalination using membrane distillation: Experimental studies on full scale spiral wound modules, J. Membr. Sci. 375 (1) (2011) 104–112.

[21] J. Swaminathan, H. W. Chung, D. M. Warsinger, J. H. Lienhard V, Membrane distillation model based on heat exchanger theory and configuration comparison, Appl. Energy 184 (2016) 491–505.

[22] D. Woldemariam, A. Martin, M. Santarelli, Exergy analysis of air-gap membrane distillation systems for water purification applications, Appl. Sci. 7 (3) (2017).

[23] H. C. Duong, P. Cooper, B. Nelemans, T. Y. Cath, L. D. Nghiem, Evaluating energy consumption of air gap membrane distillation for seawater desalination at pilot scale level, Sep. Purif. Technol 166 (2016) 55–62.

[24] J. A. Andrés-Mañas, A. Ruiz-Aguirre, F. G. Acién, G. Zaragoza, Performance increase of membrane distillation pilot scale modules operating in vacuum-enhanced air-gap configuration, Desalination 475 (2020) 114202.

[25] R. d. S. Silva, H. Ramlow, B. d. C. Santos, H. B. Madalosso, R. A. F. Machado, C. Marangoni, Membrane distillation: Experimental evaluation of liquid entry pressure in commercial membranes with textile dye solutions, J. Water Process. Eng. 44 (2021) 102339.

[26] J. A. Andrés-Mañas, I. Requena, G. Zaragoza, Membrane distillation of high salinity feeds: Steady-state modelling and optimization of a pilot-scale module in vacuum-assisted air gap operation, Desalination 553 (2023) 116449.

16

[27] A. Boubakri, A. Hafiane, S. A. T. Bouguecha, Application of response surface methodology for modeling and optimization of membrane distillation desalination process, J. Ind. Eng. Chem. 20 (5) (2014) 3163–3169.

[28] F. Ricceri, B. Blankert, N. Ghaffour, J. S. Vrouwenvelder, A. Tiraferri, L. Fortunato, Unraveling the role of feed temperature and cross-flow velocity on organic fouling in membrane distillation using response surface methodology, Desalination 540 (2022) 115971.

[29] P. Gharbani, A. Mehrizad, S. A. Mosavi, Optimization, kinetics and thermodynamics studies for photocatalytic degradation of methylene blue using cadmium selenide nanoparticles, npj Clean Water 5 (1) (2022) 34.

[30] A. Tiraferri, N. Y. Yip, A. P. Straub, S. Romero-Vargas Castrillon, M. Elimelech, A method for the simultaneous determination of transport and structural parameters of forward osmosis membranes, J. Membr. Sci. 444 (2013) 523–538.

[31] M. Hardikar, V. Felix, L. K. Presson, A. B. Rabe, L. A. Ikner, K. L. Hickenbottom, A. Achilli, Pore flow and solute rejection in pilot-scale air-gap membrane distillation, J. Membr. Sci. 676 (2023) 121544.

[32] L. Eykens, I. Hitsov, K. De Sitter, C. Dotremont, L. Pinoy, B. Van der Bruggen, Direct contact and air gap membrane distillation: Differences and similarities between lab and pilot scale, Desalination 422 (2017) 91–100.

[33] L. Chen, P. Xu, H. Wang, Interplay of the factors affecting water flux and salt rejection in membrane distillation: A state-of-the-art critical review, Water 12 (10) (2020).

[34] Z. Liu, Q. Gao, X. Lu, Z. Ma, H. Zhang, C. Wu, Experimental study of the optimal vacuum pressure in vacuum assisted air gap membrane distillation process, Desalination 414 (2017) 63–72.

[35] M. Hardikar, I. Marquez, T. Phakdon, A. E. Sáez, A. Achilli, Scale-up of membrane distillation systems using bench-scale data, Desalination 530 (2022) 115654.